09

Diagnostic of ICF target inhomogeneous compression by characteristic X-ray radiography

© A.A. Andreev[1,2], D.S. Bespalov[1¶], K.Yu. Platonov[3], M.V. Sedov[4]

[1] St. Petersburg State University,
199034 St. Petersburg, Russia
[2] Ioffe Institute,
194021 St. Petersburg, Russia
[3] Peter the Great St. Petersburg Polytechnic University,
195251 St. Petersburg, Russia
[4] Joint Institute for High Temperatures, Russian Academy of Sciences,
125412 Moscow, Russia

¶ e-mail: dmitriy.bespalov.s@gmail.com

Received March 03, 2022
Revised March 03, 2022
Accepted March 15, 2022

A scheme is considered and the parameters of a multipulse X-ray source for obtaining images of the compressed state of a primary laser thermonuclear target are determined. As an example of a source, we consider the characteristic radiation of an iron secondary target with focusing on it of several picosecond laser pulses of subrelativistic intensity. The proposed technique makes it possible to determine the relative large-scale inhomogeneity of the energy release of laser beams that irradiated the thermonuclear target, based on the results of X-ray diffraction of a compressed thermonuclear target, and to estimate the decrease in the neutron yield caused by the asymmetry of the compressed target.

Keywords: picosecond laser plasma, characteristic X-ray radiation, target in laser thermonuclear fusion, iron secondary target, backlighter image.

DOI: 10.21883/EOS.2022.06.54714.3350-21

1. Introduction

As known, the development of X-ray sources for diagnostics of dense media started with the discovery of X-ray radiation, however, study of fast enough processes with this method has only become possible fairly recently, in particular with the Advance Radiographic Capability (ARC) at the NIF (National Ignition Facility) — compression of the main target in laser thermonuclear synthesis (LTS) by its backlight imaging using X-ray pulses obtained by irradiation of the secondary target by laser pulses [1,2]. As known, there are two main methods of X-ray radiography: a point-source radiography where the X-ray source is much smaller than the target being radiographed, and an extended-source radiography where size of the source is comparable with that of the target. When a point source is used, the target image on the detector is less distorted than in the case of spatial source, albeit less quanta are arrived to the detector.

State of the target can be diagnosed using characteristic X-ray lines. In recent decades theoretic and experimental studies of the laser plasma characteristic radiation (in particular, $K\alpha$) at the interaction of short (~ 10 ps) laser pulses with different targets were conducted. By using different materials of the target, it is possible to obtain $K\alpha$-radiation with photon energies in a range of $1-100$ KeV. Numerous publications are devoted to optimization of the coefficient of laser radiation conversion to $K\alpha$-line radiation [3,4]. The maximum coefficient of conversion to $K\alpha$-radiation achieved experimentally at a length of laser pulse of ~ 1 ps is $\sim 10^{-4}$ [4]. An example of $K\alpha$-radiation source for plasma diagnostics is a $200 \times 200 \times 20\,\mu$m copper plate irradiated by subpicosecond pulse with an intensity of 10^{19} W/cm^2, with a conversion coefficient of $4 \cdot 10^{-4}$ [5].

In addition to $K\alpha$-radiation, hot laser plasma recombination lines (Ly-α and He-α) are possible sources of monochromatic X-rays as well. The practicability to use Ly-α- and He-α-radiation is connected with non-optimum parameters of the $K\alpha$-line excitation pulse for some laser systems. For example, in [6] an experimentally obtained coefficient of laser radiation conversion to He-α-line is reported to be $\sim 10^{-3}$ at a laser intensity of 10^{17} W/cm^2, which is higher than the coefficient of conversion to $K\alpha$-line at the same conditions. Another example of spatial source with high intensity of He-α-line [7] is a target in the form of $15\,\mu$m thick germanium plate irradiated by several beams of the NIF laser facility with each beam intensity of $\sim 10^{15}$ W/cm^2 and a duration of 1 ns. An electron-optical camera with a time resolution of ~ 30 ps and a spatial resolution of $\sim 10\,\mu$m made it possible, with the use of such source, to obtain a time sequence of X-ray patterns for the compressed thermonuclear target, while the coefficient of conversion to He-α-line was $\sim 5 \cdot 10^{-3}$.

Previously, in [8,9] a two-dimensional model of homogeneous laser LTS target backlight imaging by an extended X-ray source in He-α-line was developed. However, it was found in a number of experiments that consideration of a two-dimensional case is not enough for correct description of the process [10]. This is connected, above all, with the fact that spatial orientation of the target in the process of compression can vary in different planes, because an asymmetry of the target irradiation by various laser beams is possible. Also, the above-cited works did not take into account the effect of spacial dimensions of the He-α-radiation source on the image, so in this work a diagnostic scheme has been developed and calculations have been made to determine optimum parameters of the X-ray He-α-source for three-dimensional backlight imaging of a compressed state of a laser thermonuclear target with a picosecond time resolution.

2. The scheme of diagnostics

In this work, a modified scheme of X-ray diagnostics of a LTS target [2] is considered, where the role of X-ray source is played by a secondary target irradiated by several laser beams.

General scheme of the diagnostics under consideration is shown in Fig. 1. Here the laser radiation of diagnostic beams is focused by a parabolic mirror onto a secondary target, as shown with lilac lines in Fig. 1. Each diagnostic beam is focused (at an angle of γ) onto its area of the secondary target creating an X-ray pulse with a certain time delay. The assumption is that, as a result of interaction, the secondary target emits X-rays isotropically in every point.

In this work we consider the „direct compression"variant of LTS, when the primary target surface is irradiated by powerful laser beams (some of them are shown in red in Fig. 1) causing compression of the primary target. With evenly emitted laser energy on the surface of an ideal shell target, spherical compression of the target takes place, however, usually in the process of compression the spherical geometry is distorted and becomes, in particular, an ellipsoid [11,12].

Parameters of the secondary target are selected at a lower level, including, among other things, the maximum efficiency of laser radiation conversion to the characteristic He-α-radiation, which radiographs the primary target and is recorded by the detector. The thermal radiation of continuous spectrum is not taken into consideration because cut-off filters are used [13].

3. Secondary target

3.1. Characteristic radiation of the secondary target

In this work, in accordance with Fig. 1, *b*, the following model is considered: diagnostic laser beams (*3*) (with

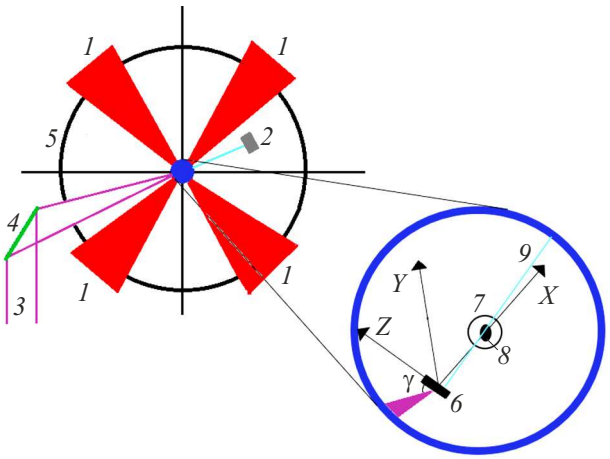

Figure 1. Scheme of X-ray diagnostics of a compressed state of a thermonuclear target. The figure shows the coordinate system used in this work. *1* — working laser beams, *2* — detector, *3* — diagnostic laser beams, *4* — parabolic mirror, *5* — vacuum chamber, *6* — secondary target, *7* — initial state of the primary target, *8* — compressed state of the primary target, *9* — radiation of the secondary target. The zoomed area illustrates the process of diagnostics of a compressed target.

super-Gaussian spatial distribution and Gaussian waveform of pulse) generally fall onto the target at a certain angle of γ (for simplicity in the following it is assumed that $\gamma = 0$). The secondary target is a metal foil with a thickness of d_0, an area of S; shown with black rectangular (*6*) in the scheme of Fig. 1. At a certain point in time of the diagnostics a laser pulse is considered, which gives information on the state of the primary target. Its duration Δt_l, quantum energy ε_l, maximum intensity $\max(I_l)$ are achieved at a moment of t_l. The area of laser spot on the secondary target is $S_1 = \pi r_f^2$, where r_f — focus spot radius. The secondary target region that emits characteristic radiation quanta has an area of $S_2 = \pi r_0^2$, where $r_0 \approx r_m + r_f$, and r_m — scale of the target surface heated by the laser. The plasma resulted from the interaction between the laser radiation and the secondary target is characterized by the following parameters: T_{el} — electron temperature and n_{el} — electron concentration. The speed of heat propagation is proportional to the thermal velocity of electrons, therefore $r_m = V_{el}\Delta t_l \approx \sqrt{\frac{3kT_e}{m_e}}\Delta t_l$, where m_e, V_{el} — mass and thermal velocity of electron. The distribution of T_{el} over the area of S_2 is assumed to be super-Gaussian.

Let us consider the X-ray emission from the secondary target. This radiation is characterized by the following parameters: J_x — intensity of emission per energy unit and ε_x — quantum energy. The characteristic radiation pulse is described by the following parameters: Δt_α — halfwidth, I_α — intensity, t_α — time to achieve maximum intensity $\max(I_\alpha)$, as well as energy of the radiation quantum — ε_α.

It should be noted that in the process of primary target backlight imaging the diagnostic laser can be turned on at any stage of the target compression, and the usage of its intensity considerably higher than $10^{17}\,\mathrm{W/cm^2}$ is unreasonable [14,15]. When selecting length of the laser pulse, it is necessary to take into account that, on the one hand, the pulse should be short enough to achieve high time resolution of the compressing target and, on the other hand, it should be long enough to obtain required density of quanta on the detector [2], which is related to characteristics of the detector. The main criterion for selection of the secondary target material is the energy of emitted characteristic quantum, because to achieve the biggest contrast of the image the primary target should absorb not more than 20% of the radiation passing through it at the moment of collapse [2]. The analysis of required quantum work and characteristic radiation intensity performed in [2,14,15] for targets made of different materials has shown that at an intensity of $\sim 10^{17}\,\mathrm{W/cm^2}$ iron has the highest coefficient of laser radiation conversion to He-α-line, therefore we use these parameters in the following study.

3.2. Results of spectral emission calculation

Let us consider the results of calculation of the secondary target spectral emission performed with the use of HELIOS 1-D radiation-hydrodynamics code [16]. Calculations were performed with the following laser parameters: $\Delta t_l = 15\,\mathrm{ps}$, $\lambda_l = 1\,\mu\mathrm{m}$, $\max(I_l) = 2 \cdot 10^{17}\,\mathrm{W/cm^2}$, the laser pulse had Gaussian waveform. The secondary target was implemented as an iron plate with a thickness of $d_0 = 20\,\mu\mathrm{m}$. The problem was solved in a planar geometry with the laser pulse normally falling onto the secondary target.

Figure 2, *a* shows the parameters of laser pulse, such as halfwidth Δt_l, maximum intensity $\max(I_l)$ at the moment of time t_l, while Fig. 2, *b* shows: Δt_α — halfwidth, I_α — intensity, and t_α — time of maximum intensity $\max(I_\alpha)$ achievement for the He-α-radiation. It should be noted that the calculated peak of He-α-radiation is shifted in relation to the laser radiation by $t_{P\alpha} - t_l = \Delta_\alpha \approx 2\,\mathrm{ps}$, and ~ 1.5 times broadened as well. The shift of the intensity peak is related to the fact that target plasma temperature and density increase with a certain delay when the target is irradiated by laser pulse [17]. The broadening of He-α-pulse in relation to the laser pulse is related to the fact that the plasma resulted from the heating keeps for a certain time the electron temperature and concentration required for X-ray emission. Figure 3 shows calculated graphs that characterize the radiation spectrum of the secondary target.

As known [18], the He-α-line of iron should lie in an energy range of $6667-6700\,\mathrm{eV}$, however, since the formed plasma has high calculated temperature and concentration ($T_{\mathrm{Fe}} \approx 6500-12500\,\mathrm{eV}$, and $n_{\mathrm{Fe}} \sim 10^{22}-10^{24}$), then the He-$\alpha$-line becomes broader due to Stark and Doppler effects [19] achieving the energy range of $\varepsilon_\alpha = 6818-7079\,\mathrm{eV}$, that can be seen in Fig. 3, *b*. These results are used to calibrate the simplified analytical model [15]. Note, that maximum emission according to the model was $I_\alpha^A = 11.22\,\mathrm{PW/cm^2}$ at the moment of time $t^{\mathrm{A}} \approx 0.101\,\mathrm{ns}$, while according to HELIOS it was $I_\alpha^{\mathrm{H}} = 15.01\,\mathrm{PW/cm^2}$ at $t^{\mathrm{H}} \approx 0.102\,\mathrm{ns}$; also, the energy of He-α-radiation pulse from an area of S_2 was $E_\alpha^{\mathrm{H}} = 3.6\,\mathrm{J}$ in HELIOS and $E_\alpha^{\mathrm{A}} = 3.46\,\mathrm{J}$ according to the model. The coefficient of laser radiation conversion to He-α-radiation for iron according to HELIOS is $\varepsilon_{kx}^{\mathrm{H}} = \frac{E_\alpha^{\mathrm{H}}}{E_l} = 0.02$ and according to the model it is $\varepsilon_{kx}^{\mathrm{A}} = \frac{E_\alpha^{\mathrm{A}}}{E_l} = 0.019$, which indicates a good accuracy (for the model of this type). However, these coefficients are calculated for the angle of 2π, and if the conversion coefficient is recalculated for the spatial angle of detector (which description is provided below) $\theta_d \approx 0.01\,\mathrm{sr}$, we get $\varepsilon_{kD} \approx 2.4 \cdot 10^{-4}$.

The number of He-α-quanta emitted by the secondary target is defined by the following relationship:

$$N_\alpha = \frac{S \int_0^{+\infty} \int_{\varepsilon_1}^{\varepsilon_2} J_x d\varepsilon_x dt}{\varepsilon_\alpha}. \qquad (1)$$

Figure 4 shows results of calculations performed by the HELIOS code for different lengths of laser pulse, all other parameters of the laser and target are given above, and $\varepsilon_\alpha = 6900\,\mathrm{eV}$. Let us define the density of X-ray quanta with an average energy of $\varepsilon_\alpha = 6900\,\mathrm{eV}$ on the detector as $\rho = \frac{N_a}{S_d}\gamma'$, where S_d — area of the detector, and γ' — its geometry factor (a spatial angle subtended at the secondary target center by the detector, divided by 4π). We assume that the detector of radiation is a CCD-matrix (with dimensions of $20 \times 20\,\mathrm{mm}$), and to perform the diagnostics, the density of quanta on the detector should be greater than the threshold level of $\rho_{\min} = 107\,\mathrm{cm^{-2}}$ (see details in [13]), then, according to Fig. 4, *b*, $\rho > \rho_{\min}$ at a length of laser pulse equal to 15 ps.

4. Primary target

4.1. Characteristics of the primary target

To describe the process of primary target compression, we select the laser and target parameters used in the experiment of [20]. In this case the target is composed of a polystyrene shell $(C_8H_8)_n$ with a thickness of $\Delta d_p = 22.6\,\mu\mathrm{m}$ and a diameter of $d_p = 939.2\,\mu\mathrm{m}$, which is filled with deuterium under a pressure of $P_{\mathrm{D}} = 10\,\mathrm{atm}$ and Ar under a pressure of $P_{\mathrm{Ar}} = 0.059\,\mathrm{atm}$, weight of the D-Ar-mixture is $m = 3\,\mu\mathrm{g}$. It is irradiated by super-Gaussian laser pulse with an intensity of $I_p = 20\,\mathrm{TW/cm^2}$ and a length of $\Delta t_p = 1\,\mathrm{ps}$, the energy of radiation quantum is equal to $\varepsilon_p = 3.54\,\mathrm{eV}$. The pulse is turned on at the moment of time $t_{\mathrm{on}} = 0.15\,\mathrm{ns}$ and turned off at the moment of time $t_{\mathrm{off}} = 1.15\,\mathrm{ns}$.

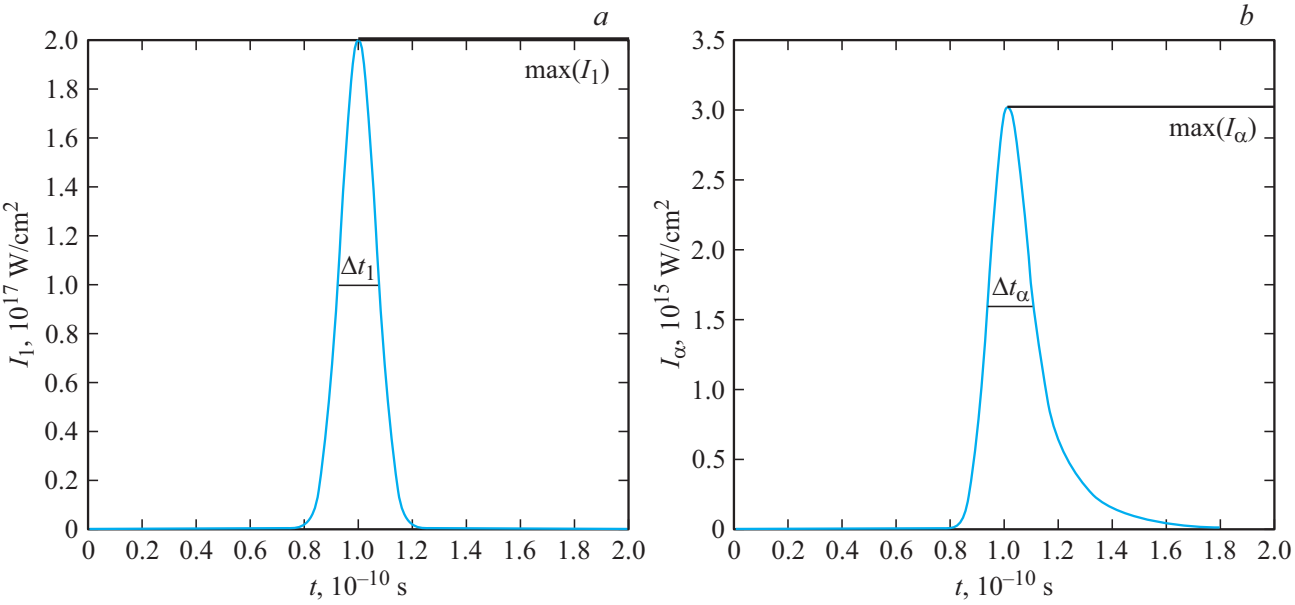

Figure 2. Pulse waveforms: a — laser radiation, b — X-ray He-α-radiation.

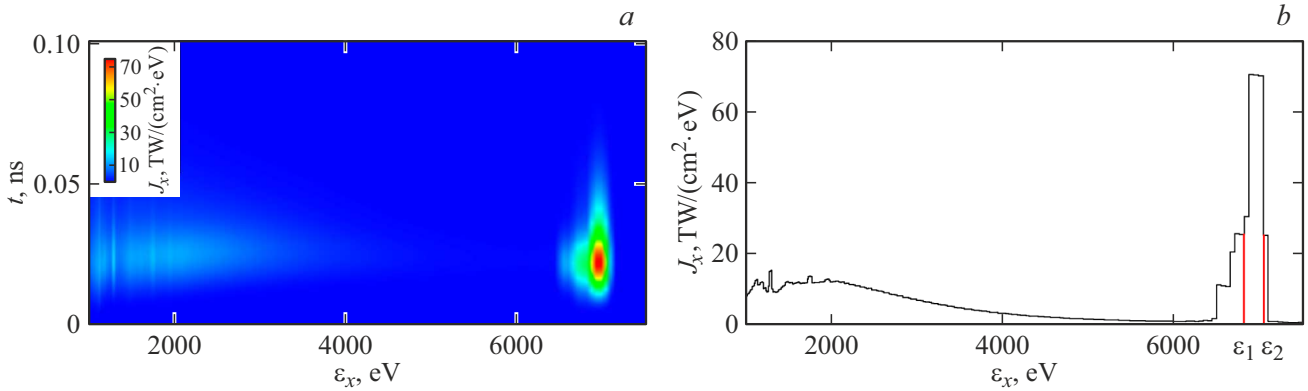

Figure 3. (a) Diagram of the emission intensity per unit energy as a function of time t_α. (b) Spectrum of the secondary target radiation $J_x(\varepsilon_x)$ at the moment of time of He-α-line maximum emission, red lines show the spectral interval $(\varepsilon_1, \varepsilon_2)$ where the line lies.

4.2. Results of calculations of primary target dynamics

To determine parameters of the primary target, we have calculated its spherical compression using the HELIOS code, because to calculate the X-ray quantum absorption by the target, a simulation is needed that makes it possible to determine parameters of the target dense part at every moment of time, such as T_e — electron temperature, n_e, n_i — concentrations of electrons and ions, respectively, as well as radius of the target dense part at every moment of time, r_d. Values of the main interest in this case are the concentrations of electrons and ions, because free length of the He-α-quantum $\sim n_e n_i T_e^{-1/2}$, temperature has less effect on the absorption than concentrations.

Note that in the process of compression until a certain moment of time it may be said that the target is approximately composed of three parts: (1) — zone of scattering shell; (2) — zone of dense compressing shell; (3) — zone of inner part of the target. Hereinafter the combination of zones (2) and (3) is referred to as the dense part of the primary target, while zone (1) is referred to as the rarefied part of the primary target. The target is compressing until the moment of time $t_k = 1.84$ ns — the time of collapse (green line on the axis in Fig. 5, a), when the target has a minimal radius, then the target starts to disintegrate. It is seen from these graphs that electron and ion concentrations before the moment of time $t = 1.7$ ns in the dense part of the target are distributed in a nonuniform manner, i.e. they differ more than an order of magnitude (Fig. 5, b). In zones (2) and (3), changes in n_e and n_i are little, which makes it possible to consider them homogeneous when solving the problems of target backlight imaging. As for the scattering shell, it is worth noting that during the compression its temperature is an order of magnitude higher

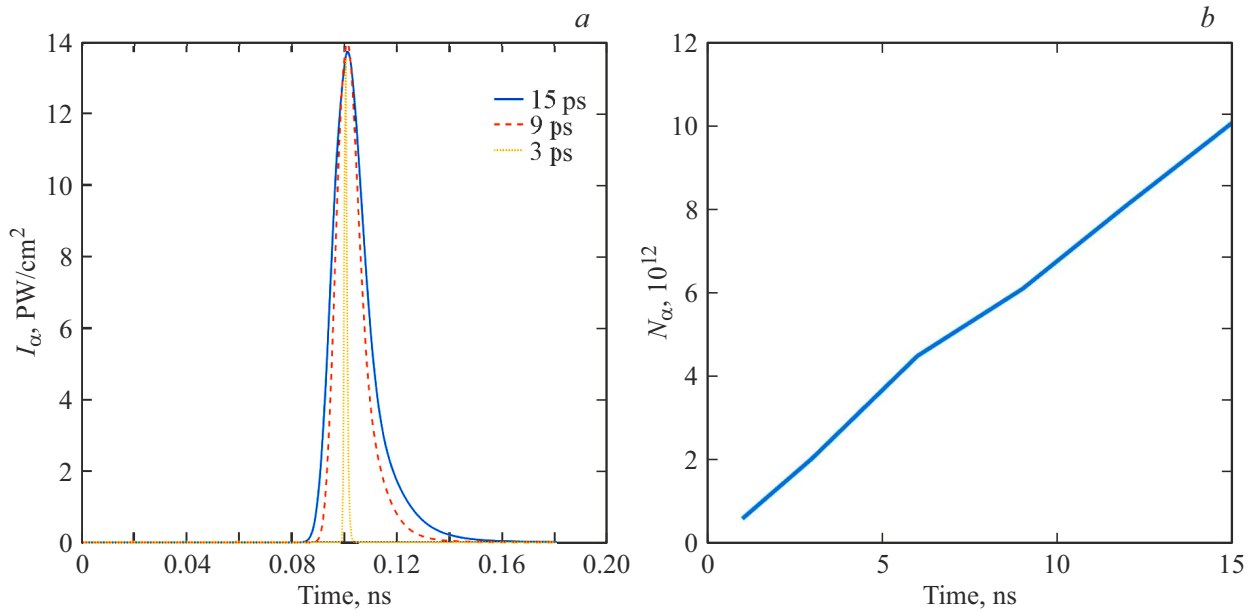

Figure 4. (*a*) Graphs of $I_\alpha(t)$ for different lengths of laser pulse. (*b*) Dependence of the number of He-α-quanta on the length of laser pulse.

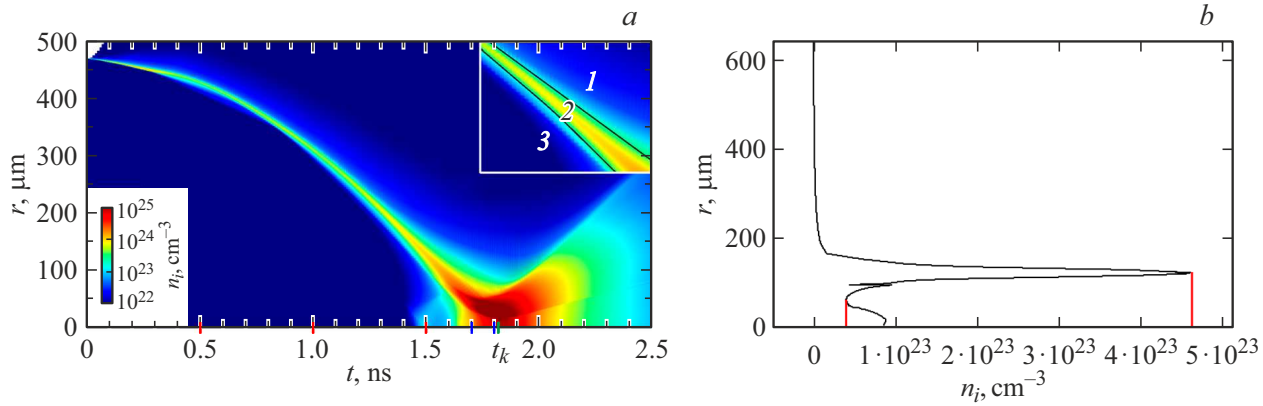

Figure 5. (*a*) Concentration of electrons n_e in the primary target as a function of time and target radius. In the top right corner a zoomed part of the graph is shown. (*b*) Graph of $n_i(r)$ at the moment of time $t = 1.5$ ns. Red lines show maximum and minimum concentration of ions in the dense part of the target.

than that in the dense part of the target, while the electron and ion concentrations are two orders of magnitude lower than those in the dense part of the target. On the basis of the absorption law, these facts allow us to ignore zone (1) in the backlight imaging of the primary target. Also, a conclusion can be made that at moments of time before $t = 1.7$ ns the target can be considered anisotropic, being composed of zones (2) and (3). At moments of time after $t = 1.7$ ns and until $t_k = 1.84$ ns the target can be considered isotropic, because it is homogenous in terms of electron and ion densities. The dynamics of zone (2) compression can be approximated by a polynomial of degree four:

$$r_d(t) = 206.1t^4 - 472.3t^3 + 189.1t^2 - 197.1t + 432.5. \quad (2)$$

4.3. The case of elliptical compression of the primary target

As known, in the process of compression of the primary target large-scale distortions are possible due to heterogeneity of the irradiation by laser beams or heterogeneity of the shell manufacturing, which results in deformation of the target in the process of compression, i.e, in deviation from the spherical shape. The experimental data and numerical models show [13,21] that the asymmetry of target compression results in a decrease in plasma density and, as a consequence, decrease in the neutron outcome. To take into account this effect, we assume that at the initial moment of time the target has a shape of sphere, but in the process of compression one of its axes starts compressing slower

than another, which causes the target to take an elliptical shape. Describing this ellipsoid, we assume that at every moment of time its volume is equal to the volume of the compressing sphere from the HELIOS-calculation. Then, an equation can be written for the change in semi-axes of the ellipsoid: $a(t)$, $b(t)$, $c(t)$ (where $a(t) = r_d(t)$):

$$\frac{4}{3}\pi r^3 = \frac{4}{3}\pi acb, \quad r^2 = cb. \tag{3}$$

Then, we assume that $b = c + \Delta c$, where Δc — a parameter that characterizes the deviation of target shape from sphere, then

$$r^2 = c^2 + c\Delta c, \; c = \frac{(\Delta c^2 + 4r^2)^{1/2}}{2} - \frac{\Delta c}{2},$$

$$b = \frac{(\Delta c^2 + 4r^2)^{1/2}}{2} + \frac{\Delta c}{2},$$

where the dependence of $r_d = r_d(t)$ is known from numerical calculations (see, for example, (2)), and $\Delta c \ll c$.

In [22] the direct compression of an LTS target with parameters similar to those of para. 4.1 was considered. In the course of experiment [22] it was found that the target compresses elliptically. The dependence of ellipse parameters on time was determined; based on this dependence a value of the Δc was selected to ensure maximum accuracy of the approximation of ellipse parameters dependence on time.

5. Modelling the primary target backlight imaging

The sequence of diagnostics processes takes place in the following order: at the initial moment of time t_{on} the primary target is irradiated by the main laser beams. After that the target starts to compress until t_k — the time of collapse. In the time interval between t_{on} and t_k the diagnostic laser is turned on. This laser irradiates the secondary target causing it to emit He-α-quanta at a moment of time $t_{\text{He}}^{\text{on}}$, which is considered as the moment of diagnostics beginning, and after the diagnostics ends up at the moment of time $t_{\text{He}}^{\text{off}}$, $t_{\text{He}}^{\text{off}} - t_{\text{He}}^{\text{on}} = \Delta t_\alpha$. To build up a mathematical model of the compressed target backlight imaging, we introduce in Fig. 6 (the zoomed fragment of Fig. 1) a central optical coordinate system where the secondary target is positioned normal to OX.

The scheme in Fig. 6 shows an example of beam outgoing from the target point T and directed to the point T'. Here ξ_1 — the secondary target, $KK'PP'$ — its boundary points, point O — the center of the secondary target and origin of the Cartesian coordinate system, T — an example of radiating point on the surface of the secondary target, (m, n) — coordinates of the radiating point on the surface of the secondary target in the coordinate system of the secondary target; ξ_2 — the primary target represented by an ellipsoid with its center at the point O', $CC' = a$,

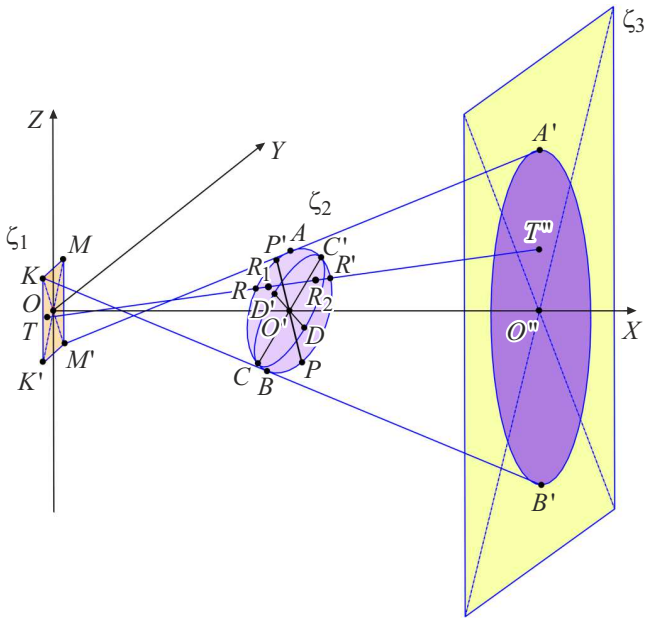

Figure 6. Optical scheme of diagnostics. Explanations in the text.

$PP' = b$, $DD' = c$ — lengths of ellipsoid axes, $\beta_1, \beta_2, \beta_3$ — tilt angles of ellipsoid axes in relation to OX, OY, OZ axes, respectively, R, R' — points of crossing between the beam, outgoing from the point T of the secondary target, and the primary target; ξ_3 — plane of the detector, O'' — its center, $A'B'$ — boundary points of the image on the detector, $T'(M, N)$ — point of arrival of the partially absorbed radiation from the point $T(y, z)$ — coordinates of the detector point passed by the partially absorbed radiation in the coordinate system of the detector plane, where (M, N) — the rectangular coordinate system related to the center of detector, $N||KK'$, $M||KP$, $KK' = KP = 200\,\mu$m.

To evaluate the radiation absorption by the primary target, we introduce l — the length of the beams section passed through the target. In the case of isotropic parameters over the entire volume of the target:

$$l = |\overline{RR'}| = |\overline{RR'} + \overline{TR'}|. \tag{4}$$

At initial stages of the primary target compression, the density and temperature of its shell are much higher than the density and temperature in its center; in this case the target can not be considered as isotropic. Therefore we assume that the target is composed of two layers. R_1 and R_2 are points of crossing between the beam outgoing from the secondary target and the inner part of the primary target. In this approximation the length of beam section has the following form:

$$l_c = |\overline{RR_1}| + |\overline{R_1R_2}| + |\overline{R_2R'}|,$$

where $|\overline{RR_1}|$ and $|\overline{R_2R'}|$ — section lengths of the beam passed through the dense shell, $|\overline{R_1R_2}|$ — section length of the beam passed through the rarefied part of the target.

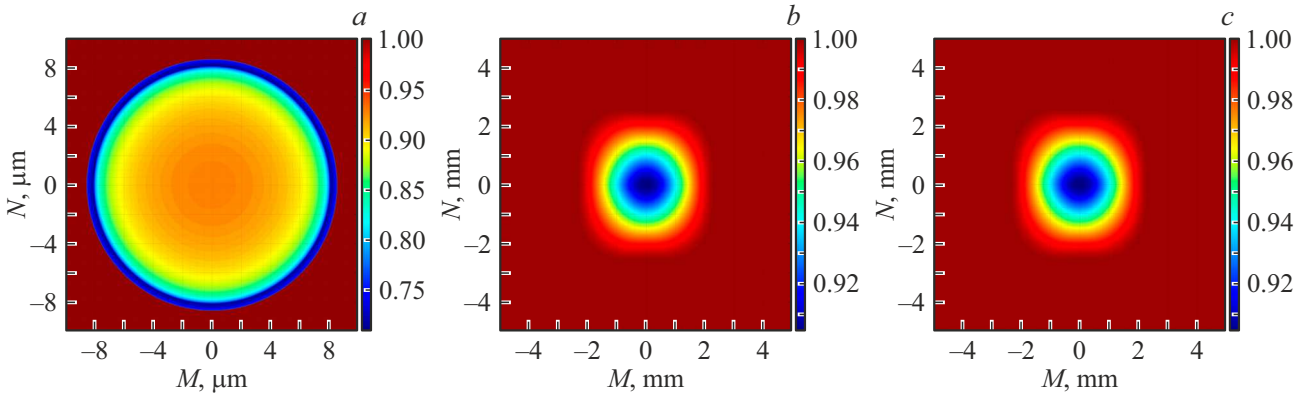

Figure 7. Target image at the following moments of time: (a) — $t = 0.5$ ns, (b) — $t = 1.8$ ns, (c) — $t_k = 1.84$ ns. At these moments of time (a) — $S_2/S_s \ll 1$, (b) — $S_2/S_s \sim 0.5$, (c) — $S_2/S_s \sim 1$ respectively.

In the considered approximation the target absorbs the X-ray radiation according to the law of [8], and the passed-through radiation is defined by the following expression:

$$I_d = I_\alpha(t) e^{\frac{-l(t,n,m,M,N,\beta_1,\beta_2,\beta_3)}{l_{\text{ph}}(t)}}. \qquad (5)$$

Here I_d — intensity arrived to the unit segment of detector from the unit area of the secondary target, $l_{\text{ph}}(t)$ — free length of the He-α-quantum in the target, and $l(t, n, m, M, N, \beta_1, \beta_2, \beta_3)$ is determined by formula (4). Averaged free length is defined by the following expression:

$$l_{\text{ph}}^{-1}(t) = l_{\text{ph}_1}^{-1}(t) + l_{\text{ph}_2}^{-1}(t).$$

Here [21]

$$l_{\text{ph}_1}^{-1} = \frac{4}{3}\left(\frac{2\pi}{3mkT_e}\right)^{1/2} \frac{e^6 Z^2 n_e n_i}{\square c m \nu^3}$$

— the absorption coefficient related to free-to-free transitions, while $l_{\text{ph}_2}^{-1} = n_e 6.65 \cdot 10^{-25}$ — the absorption coefficient related to the Thomson scattering, where T_e — electron temperature and n_e, n_i — concentration of electrons and ions, respectively, ε_α — energy of radiation quantum, Z — atomic number of the element. Then

$$l_{\text{ph}}^{-1} = 1.94 \cdot 10^{-28} \frac{n_e n_i}{\sqrt{T_e}\varepsilon_\alpha^3} + 6.65 \cdot 10^{-25} n_e. \qquad (6)$$

Using the Matlab software package a numerical model was created associating each point of the screen with the intensity arrived to this point over the time interval from t_0 to t_e, where t_0 — start time of the observation, t_e — end time of the observation.

Based on the study of quantum absorption by the primary target the $\frac{I_d}{I_\alpha}(\varepsilon_x)$ dependence at the moment of collapse was determined, where $\frac{I_d}{I_\alpha}$ is the ratio between intensities of the He-α-radiation passed through the primary target and the intensity of unabsorbed He-α-radiation. According to (5), when $\varepsilon_\alpha = 6900$ eV, the absorption by the primary target is low ($\sim 12.5\%$), therefore iron can be used as a material of the secondary target.

In the process of work the program created in the Matlab software splits to radiating plane $KPK'P'$ into N_s point sources of X-ray radiation, each having an energy at a certain moment of time equal to $\Delta I_\alpha = \frac{I_\alpha(t)}{N_s}$. Then for each source at every moment of time a distribution of intensity $I(M, N)$ is determined, where (M, N) is coordinate of the detector point ξ_3, each point is associated with a radiation intensity, arrived to this point from each point source,i.e. formula (5) is integrated numerically (summed) for (y, z) — coordinate of the source in the range of its dimensions:

$$P_d(M, N) = \sum_{y=y_0}^{y_1} \sum_{z=z_0}^{z_1} \Delta I_\alpha(y, z, t) \times \exp\left[\square - \frac{l(t, n, m, M, N, \beta_1, \beta_2, \beta_3)}{l_{\text{ph}}(t)}\right],$$

where $P_d(M, N)$ — the radiation power arrived to the point of detector with a coordinate of (M, N), (y_0, z_0), (y_1, z_1) — coordinates of points bounding the radiating area. Then the above expression is integrated for time and the energy arrived to the detector is yielded:

$$E_d(M, N) = \int_{t_{\text{He}}^{\text{on}}}^{t_{\text{He}}^{\text{off}}} \sum_{y=y_0}^{y_1} \sum_{z=z_0}^{z_1} \Delta I_\alpha(y, z, t) e^{\frac{-l(t,n,m,M,N,\beta_1,\beta_2,\beta_3)}{l_{\text{ph}}(t)}} dt. \qquad (7)$$

Here $E_d(M, N)$ is the energy of partially absorbed radiation arrived to the detector point with a coordinate of (M, N). It should be noted that to calculate values of $l_{\text{ph}}(t)$, the dependencies of averaged values of electron and ion concentrations and temperature were approximated (on the basis of HELIOS calculation, using spline function) for each of target layers. This code was implemented in the Matlab software package. To accelerate calculations, the code to calculate expression (7) was optimized. The technologies of parallel programming and calculation of matrix products with GPU (Graphics Processing Unit) used in the code allowed shortening the time of its execution by 6 times.

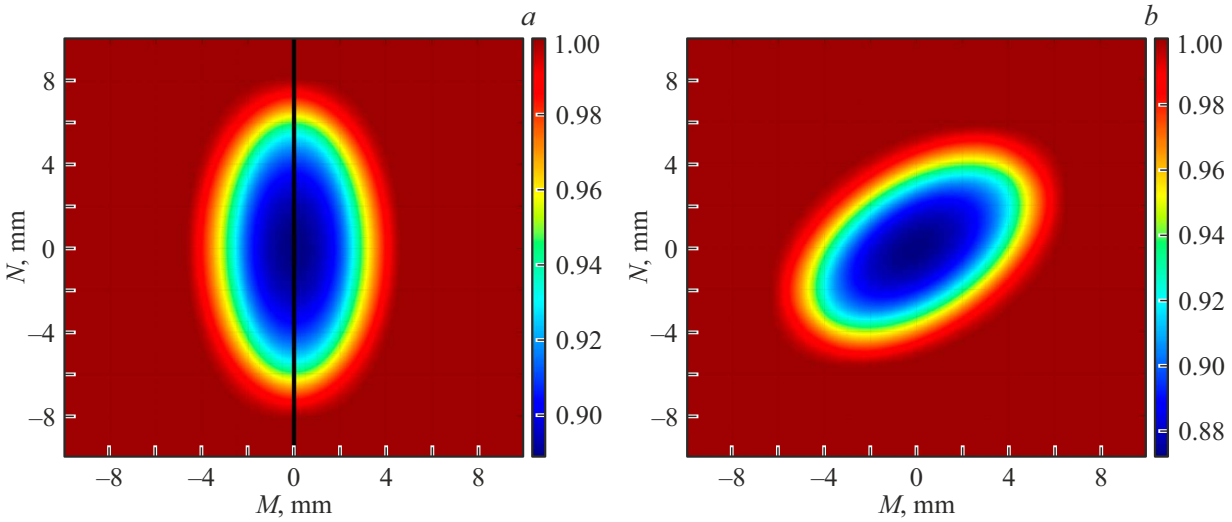

Figure 8. Target image at (a) — $\beta_1 = \beta_2 = \beta_3 = 0$, (b) — $\beta_1 = \beta_2 = \beta_3 = \pi/4$.

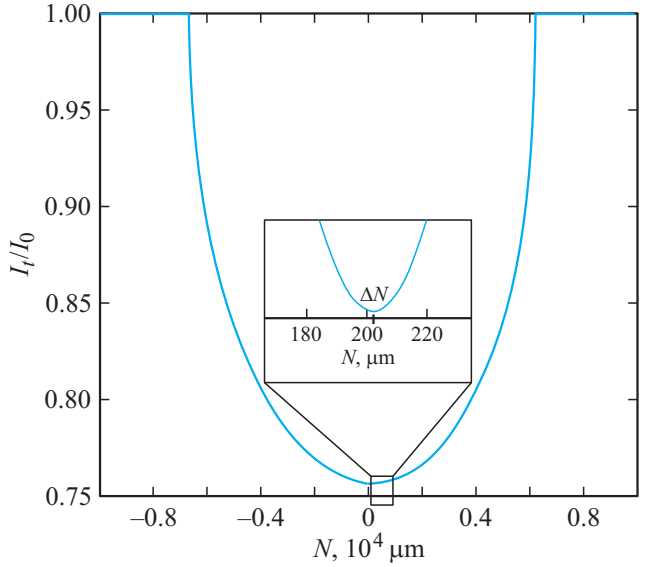

Figure 9. Intensity distribution over the plane of detector in case of the simplified model, I_t/I_0 — normalized intensity of the laser radiation at the detector, 0 — coordinate of the detector center, N — coordinate of the point at the detector; the black rectangular shows zoomed intensity distribution of the partially absorbed radiation at the detector; ΔN — coordinate of intensity minimum.

5.1. Results of the primary target backlight imaging

The modelling of the primary target backlight imaging yields the spatial distribution of the partially absorbed energy of the laser radiation achieved the detector plane, which hereinafter is referred to as the image. Let us consider the model images obtained on the detector screen in the case of density-inhomogeneous primary target at the moments of time marked with red lines in Fig. 5, *a*. The detector of radiation is the plane of ξ_3 (Fig. 6), a coordinate system is introduced on the detector with axes (M, N), which is described in the previous section as well.

Figure 7, *a* shows the ring-shaped image for a single-layer primary target for an early moment of time. This shape is caused by the fact that the dense part of the target absorbs several times more He-α-radiation than its inner part. Next (Fig. 7, *b, c*) quasi-ring images are modelled that are obtained on the detector screen (in the case of the same target) at the moments of time marked with the first blue line in Fig. 5, *a*, as well as at the moment of collapse (green line). The last figure shows heavy distortions of the image shape (ring) caused by the effect of geometrical dimensions of the secondary target. Since the radiating spot has an area of $S_2 = 10^4\,\mu\text{m}^2$, the primary target is small in comparison with the radiating spot until the area of its section by the plane normal to OX axis and passing through its geometrical center is much greater (i.e. $S_2 \ll S_s$) than $S_s = \pi bc$ — the cross-section area of the primary target. This condition is met until the moment of time $t = 1.5$ ns, and after this moment the secondary target is no longer a point-source as compared with the primary target.

5.2. Image of the primary target in case of elliptical compression

Figure 8 below shows as an example the model images of the target with an axes ratio of $a : b : c = 1 : 4 : 8$, rotated by different angles $\beta_1, \beta_2, \beta_3$.

5.3. Features of the image obtained through backlight imaging of a target having a geometry of inclined ellipse

In the process of analysis of the obtained model images, it was found that minimum of the passed-through intensity is shifted in relation to the center of detector (the point

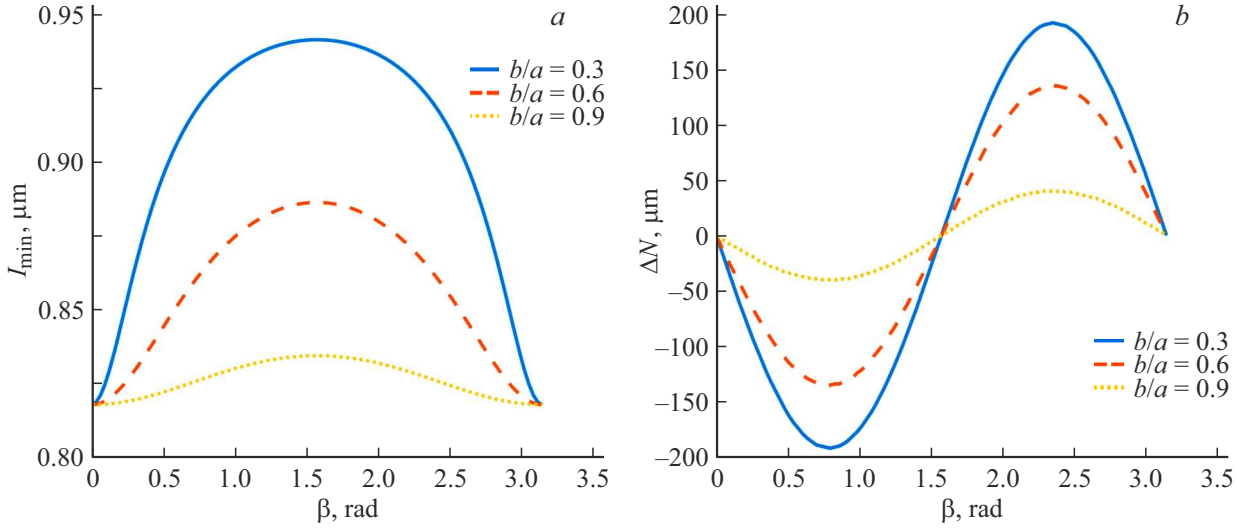

Figure 10. (a) Approximation of the minimum intensity shift dependence on the target tilt, where ΔN — shift of the minimum of passed through intensity along the N axis, (b) — dependence of the intensity minimum on the rotation angle of the primary target.

of $N = 0$, $M = 0$, $\beta_1, \beta_2, \beta_3 \neq \pi n/2$, where n is a natural number). To study the shift of minimum of the passed-through intensity, let us consider a section of the diagnostic scheme shown in Fig. 6 by a plane. This scheme illustrates the shift of absorption minimum. Let as consider the image of intensity distribution over the detector (plane ξ_3) in case of 2D scheme of diagnostics, when the intensity distribution is a section of Fig. 8, a along the N axis (black line). To illustrate the shift under consideration, we represented the yielded section of image in Fig. 9. Then we fixed the ratio of a/b and started vary the tilt angle of the ellipse β_1 from 0 to π. Figure 10 shows the change in coordinate ΔN and the value of $I_{\min}$ under this variation.

Thus, based on the data of the images on the detector at a certain moment of time (from the dependencies in Fig. 10, a, b) the following system of equations can be written:

$$\begin{cases} \Delta N = \Delta N(\beta_1, \xi), \\ I_{\min} = I_{\min}(\beta_1, \xi). \end{cases} \tag{8}$$

Here $I_{\min} = \min\left(\frac{I_L}{I_0}\right)$, ΔN — the data obtained from the images, $\xi = \frac{b}{a}$. By solving this system, for example, in the rotation angle of target, the angle of β_1 can be determined at known values of $\min\left(\frac{I_L}{I_0}\right)$ and $\Delta N(\beta_1, \xi)$. It is seen from the performed modelling that

$$\Delta N \approx C(\xi)\sin(2\beta + \pi), \quad I_{\min} \approx A(\xi)\exp\left(-\left(\frac{\beta - \frac{\pi}{2}}{D(\xi)}\right)^2\right),$$

and this approximation is applicable for $a, b \in (50, 1000)\,\mu$m, and coefficients of the approximation can be yielded by the Taylor?s expansion of a function of two variables. For a quadratic approximation we get:

$$C(\xi) = -16.6\xi^2 - 62\xi + 152.6,$$

$$A(\xi) = 0.7\xi^2 + 1.2\xi^2 + 4.6,$$

$$D(\xi) = 0.01\xi^2 - 0.7\xi + 0.9$$

at $a = 1000\,\mu$m, $b \in (300, 900)\,\mu$m. Hence, with known values of $I_{\min}$ and ΔN, by solving system (8) parameters of the ellipsoid can be determined, and then the large-scale inhomogeneity of the target irradiation by laser beams can be found. Note that even a large-scale asymmetric compression of a target can reduce considerably the neutron output at the LTS. For example, according to [23], the dependence of neutron output on the degree of compression inhomogeneity ξ can be written as follows:

$$Y \approx Y_0\left\{1 - [(1-\xi)/(1+\xi)]^2\right\}^{3.3},$$

then with the asymmetry considered in this work, the neutron output is reduced by ~ 2 times. However, it is known that in some experiments [22] ξ can be ~ 0.1, and in this case the neutron output decreases by 10^2, which effects significantly on the LTS behavior.

If a large-scale target compression inhomogeneity (ellipsoid instead of sphere) is detected by the diagnostics under consideration, it is useful to determine possible averaged directions (zones) of inhomogeneous irradiation by multiple laser beams in order to further check their parameters. In this case, by solving system (8), it is possible to determine the angles of arrival of the radiation with the highest and the lowest intensity to the primary target: $\varphi_1 = \beta_1$ — angle of arrival of the lowest intensity radiation, and $\varphi_2 = \beta_1 + \frac{\pi}{2}$ — angle of arrival of the highest intensity radiation. Using section of Fig. 7, b by a straight line passing through the point (0,0) and parallel to the coordinate axis N, ΔN^1 and $I^1_{\min}$ can be obtained, and by solving system (8), we get solutions: $\beta = \beta_1 = 0$ and $\xi = \xi_1 = 0.46$. As known [21], the evaluation of large-scale inhomogeneity of the laser beams energy emission $\alpha = q_1/q_2$ depending on

the rates of ellipsoid semi-axes compression can be written as follows: $\alpha = (u_1/u_2)^3$, where $q_{1,2}$ — the energy absorbed by fast and slow moving parts of the target, respectively, while $u_1 = \frac{da}{dt} > u_2 = \frac{ddb}{dt}$ — rates of ellipsoid semi-axes compression obtained by time differentiation of (2) and (3). It should be noted that in our conditions (Fig. 7) $\alpha \sim 0.1$, and this allows us to use the above-mentioned averaging.

Let us estimate the measurement of target parameters over the time of laser pulse passage through it. The calculations of the average rate of target compression at a moment of time close to the collapse yielded $V \approx 10^7$ cm/s, while radius of the primary target was $r_{av} \approx 10^{-2}$ cm, then, assuming that He-α-quanta propagate with the speed of light, we estimate the change in target radius over the time of quantum passage through it as $\Delta r_1 = (r_{av}/c)V = t_{av}V \sim 10$ nm, where $t_{av} \approx 3.33$ ps — time of radiation quantum passage through the primary target. Taking into account length of the laser pulse irradiating the secondary target, time resolution of the diagnostics is ~ 20 ps. Using the formula to calculate resolution of detector [8], we get that in the center of detector the resolution is minimal and equal to $\Delta r_{2\,\min} \approx 15\,\mu$m, and at the edges of the primary target image the resolution is maximal and equal to $\Delta r_{2\,\max} \approx 0.1\,\mu$m.

6. Conclusion

In this work a scheme is considered and parameters are determined for a multipulse X-ray source to obtain images of the compressed state of a laser thermonuclear target, and a mathematical model of source functioning is created. An example of such source can be He-α-radiation of an iron limited secondary target with several laser pulses focused on it with an intensity of $2 \cdot 10^{17}$ W/cm^2 and a length of 15 ps. Spatial resolution of such source is $\sim 15\,\mu$m, and its time resolution is ~ 20 ps.

With the X-ray diagnostics of a primary compressed target it is found that if the target turns to the geometry of an ellipsoid rotated by a certain angle in relation to the main optical axis, the minimum of passed through intensity on the detector is shifted in relation to the place where it is located in case of spherical target. The procedure constructed in this work makes it possible to use the shift of the minimum to determine parameters of the primary target such as the ratio of its semi-axes lengths („nonsphericity “ of the compression), as well as the tilt angle of the ellipsoid in relation to the main optical axes. Also, in this work distortions of the primary target images are investigated when the target obtains a small radius (as compared with size of the secondary target) as a result of compression.

Thus, the suggested procedure makes it possible to determine the relative inhomogeneity of energy emission from the laser beams irradiated the primary target on the basis of results of X-ray radiography of the compressed thermonuclear target, and to estimate the decrease in neutron output caused by the asymmetry of the compressed target, which allows correction of parameters of the experimental setup to obtain spherically symmetric compressed states, as well as the highest compression coefficient and neutron output, respectively.

Conflict of interest

The authors declare that they have no conflict of interest.

References

[1] G. A. Kyrala, S. Dixit, S. Glenzer, D. Kalantar et al. Rev. Sci. Instrum., **81**, 10E316 (2010). DOI: 10.1063/1.3481028
[2] A.A. Andreev, S.A. Bel'kov, K.Yu. Platonov, V.V. Romanov, G.S. Rogozhnikov. Opt. Spectrosc., **123** (3), 471 (2017).
[3] B. Soom, H. Chen, Y. Fisher, D.D. Meyerhofer. J. Appl. Phys., **74**, 5372 (1993). DOI:10.1063/1.354240
[4] D. Babonneau, M. Primout, F. Girard et al. Phys. Plasmas, **15**, 092702 (2008). DOI: 10.1063/1.2973480
[5] W. Theobald et al. Phys. Plasmas, **17**, 103101 (2010). DOI: 10.1063/1.3484217
[6] M.J. Ayers, B. Felker, V. Smalyuk et al. In: *SPIE Conference San Diego* (CA, United States August 12, 2012).
[7] J. Lindl, O. Landen, J. Edwards. Phys. Plasmas, **21**, 020501 (2014). DOI: 10.1063/1.4865400
[8] A.A. Andreev, D.S. Bespalov, M.V. Sedov, K.Y. Platonov. In: *2020 International Conference Laser Optics* (ICLO, 2020), v. 1. DOI: 10.1109/ICLO48556.2020.9285849
[9] D.S. Bespalov, M.V. Sedov, K.Y. Platonov, A.A. Andreev. In: *DDFIW2021* (Prague, 2021).
[10] H.-K. Chung, M.H. Chen, W.L. Morgan, Y. Ralchenko, R.W. Lee. High Energy Density Physics, **1**, 3 (2005). DOI: 10.1016/j.hedp.2005.07.001
[11] B. Cheng, T.J.T. Kwan, S.A. Yi, O.L. Landen, Y.M. Wang, C.J. Cerjan, S.H. Batha, F.J. Wysocki. Phys. Rev. E, **98**, 023203 (2018). DOI: 10.1103/PhysRevE.98.023203
[12] J. Lindl et al. Phys. Plasmas, **11**, 339 (2004). DOI: 10.1063/1.1578638
[13] S. Glenn, P.M. Bell, L.R. Benedetti et al. In: *Proceedings of the International Conference on Accelerator and Large Experimental Physics Control Systems* (ICALEPCS, San Francisco, 2013).
[14] D. Riley, N.C. Woolsey, D. McSherry et al. Plasma Sources Sci. Technol., **11**, 484 (2002). DOI: 10.1088/0963-0252/11/4/315
[15] M.V. Sedov, K.Yu. Platonov, A.A. Andreev. Opt. and spectr., **125** (6), 734 (2018). DOI: 10.21883/OS.2018.12.46931.183-18
[16] J.J. MacFarlane, I.E. Golovkin, P.R. Woodruff. J. Quantitative Spectroscopy and Radiative Transfer, **99** (1−3), 381 (2006). DOI: 10.1016/j.jqsrt.2005.05.031
[17] T.Q. Qiu, C.L. Tien. Intern. J. Heat and Mass Transfer, **35** (3), 719 (1992).
[18] A. Kramida, Yu. Ralchenko, J. Reader et al. NIST Atomic Spectra Database (ver. 5.9), [Online]. https://physics.nist.gov/asd [2021, November 21]. (National Institute of Standards and Technology, Gaithersburg, MD). DOI: 10.18434/T4W30F
[19] N. Konjević. Phys. Rep., **316** (6), 339 (1999). DOI: 10.1016/S0370-1573(98)00132-X

[20] R.L. McCrory, R.E. Bahr et al. OMEGA ICF Experiments and Preparation for Direct-Drive Ignition on NIF, International Nuclear Information System, Nuclear Fusion. 41. 1413. DOI: 10.1088/0029-5515/41/10/309
[21] A.A. Andreev, A.A. Mak, N.A. Solovyev. *An introduction to hot laser plasma physics* (Nova Science Publishers, Huntington, 2000).
[22] R.S. Craxton, K.S. Anderson, T.R. Boehly, V.N. Goncharov et al. Phys. Plasmas, **22**, 110501 (2015). DOI: 10.1063/1.4934714
[23] N.G. Basov, I.G. Lebo, V.B. Rozanov, *Physics of the Laser Thermonuclear Synthesis* (Znaniye, M., 1988).